J. Fluid Mech. (2007), *vol.* 591, *pp.* 437–459.
doi:10.1017/S0022112007008348 Printed in the United Kingdom

Ion evaporation from Taylor cones of propylene carbonate mixed with ionic liquids

I. GUERRERO[1], R. BOCANEGRA[1], F. J. HIGUERA[2] AND J. FERNANDEZ DE LA MORA[1]

[1]Yale University, Mechanical Engineering, New Haven, CT 06520-8286, USA

[2]E. T. S. Ingenieros Aeronáuticos, UPM, Pza. Cardenal Cisneros 3, 28040 Madrid, Spain

(Received 10 February 2005 and in revised form 15 July 2007)

A combined experimental and numerical approach is used to extract information on the kinetics of ion evaporation from the region of high electric field around the tip of a Taylor cone of the neutral solvent propylene carbonate (PC) mixed with two ionic liquids. On the numerical side, the electric field on the surface of the liquid is computed in the absence of evaporation by solving the electrohydrodynamic problem in this region within the framework of the leaky dielectric model. These computations justify the approximate (2% max error) scaling $E_{max} = \beta E_k$ for the maximum electric field on the surface, with $E_k = \gamma^{1/2}\epsilon_0^{-2/3}(K/Q)^{1/6}$ for $0.111 < K < 0.888\,\mathrm{S\,m^{-1}}$ and a numerical value of $\beta \approx 0.76$. Here γ is the surface tension of PC, ϵ_0 is the electrical permittivity of vacuum, and K and Q are the liquid electrical conductivity and flow rate. On the experimental side, 16 different propylene carbonate solutions with either of the ionic liquids 1-ethyl-3-methylimidazolium tetrafluoroborate (EMI-BF_4) or EMI-bis(trifluoro-methylsulfonyl)imide (EMI-Im) are electrosprayed in a vacuum from a single Taylor cone, and their emissions of charged drops and ions are analysed by time-of-flight mass spectrometry at varying liquid flow rates Q. The sprays contain exclusively drops at large Q, both for small and for large electrical conductivities K, but enter a mixed ion–drop regime at sufficiently large K and small Q. Interestingly, the mixtures containing 10 % and 15 % (vol) EMI-Im exhibit no measurable ion currents at high Q, but approach a purely ionic regime (almost no drops) at small Q. The charge/mass ratio for the drops produced in these two mixtures increases continuously with decreasing Q, and gets very close to ionic values. Measured ion currents are represented versus computed maximum electric fields E_{max} on the liquid surface to infer ion evaporation kinetics. Comparison of measured ion currents with predictions from ion evaporation theory yields an anomalously low activation energy ($\sim$1.1 eV). This paradox appears to be due to alteration of the pure cone–jet electric field in the scaling laws used for the pure cone–jet regime, due to the substantial ion current density arising even when the ion current is relatively small. Elimination of this interference would require future ion current measurements in the 10–100 pA level. The electrical propulsion characteristics of the emissions from these liquids are determined and found to be excellent, particularly for 10 % and 15 % (vol) EMI-Im.

1. Introduction

A meniscus of an electrically conducting liquid subject to a high voltage relative to surrounding electrodes can be a very useful source of electrically charged drops, which often have relatively narrow size distributions. Cloupeau & Prunet-Foch (1989,

1990, 1994) carried out extensive experiments and compiled a catalogue of observed modes of operation of these sources. Foremost among these modes for its practical importance is the so-called cone–jet mode, which is achieved when the interface between the conducting liquid and a gas (Zeleny 1917; Taylor 1964) or an insulating liquid (Barrero *et al.* 2004) is charged above a certain critical voltage. The meniscus then evolves into a conical shape (a Taylor cone) whose tip ejects a narrow jet which eventually breaks into a spray of monodisperse drops; see Fernandez de la Mora (2007) for a review. Recent work aimed at determining the scaling laws that give the electric current and the size of the drops as functions of the flow rate injected through the meniscus and the properties of the liquid, as well as to ascertain the limits of operation of the cone–jet mode, has been carried out by Fernandez de la Mora *et al.* (1990), Fernandez de la Mora & Loscertales (1994), Gañán-Calvo, Dávila & Barrero (1997), Cherney (1999), and Higuera (2003*a*), among others. Gañán-Calvo (1997, 1999, 2004) has proposed a suite of scaling laws relying on different assumptions and levels of description, presumably applicable to different regimes of functioning of the devices. It is unfortunately not clear from these papers under what conditions each of these various models should be preferred over the others. An electric current proportional to the square root of the flow rate is a finding common to many of the cited works, but slight differences exist in the theoretical predictions of the size of the drops, which experiments have not confirmed yet (see, e.g., Chen & Pui 1997 and Gamero-Castaño & Hruby 2002).

The diameter of the jet (and therefore the size of the drops) decreases when the flow rate decreases or the electrical conductivity of the liquid increases. Depending on the values of these parameters, the jet diameter can be made rather small, down to about 10 nm (Fernandez de la Mora & Loscertales 1994). This singular ability to atomize liquids into nearly uniform drops of such small sizes has led to a number of interesting applications. In some, such as in electrical propulsion, even smaller drops would be preferred (Bocanegra, Fernandez de la Mora & Gamero-Castaño, 2004). However, a new effect interferes when trying to produce increasingly narrow jets, as the maximum electric field E_{max} on the surface of the cone–jet increases with decreasing jet diameter. Eventually, E_{max} reaches values in the range of 1 $\mathrm{V\,nm^{-1}}$, sufficient for ion evaporation to occur. This new phenomenon then changes drastically the structure of the meniscus tip, in a fashion that remains poorly understood, and whose study is the objective of the present paper.

Evidence for ion evaporation from electrified liquid cones formed in a vacuum has been available for a long time in a variety of settings. They have included metal ion evaporation from Taylor cones of liquid metals (Prewett & Mair 1991), solute ion evaporation from electrolytes of glycerol held at very high voltage in the multi-cone 'rim emission' mode (Cook 1986; Huberman 1970; Huberman & Rosen 1974; Martinez-Sanchez *et al.* 1999), ion evaporation from single Taylor cones of highly conducting materials such as sulphuric acid (Perel *et al.* 1969), electrolytes of formamide (Gamero-Castaño & Fernandez de la Mora 2000*b*; Gamero-Castaño & Hruby 2001; Bocanegra *et al.* 2004) and molten salts (Romero-Sanz *et al.* 2003; Romero-Sanz & Fernandez de la Mora 2004; Lozano 2003; Lozano & Martinez-Sanchez 2005).

Liquid-metal ion sources are of considerable scientific and technological interest, and have been studied in most detail. They differ drastically from the other cases mentioned above in that, due to the high electrical conductivity of liquid metals, the meniscus behaves essentially as an equipotential surface (Higuera 2004 and references therein). As a result one has no substantial experimental control on the electric field on the meniscus surface other than by acting on the applied voltage, and thus it

is difficult to infer information on the kinetics of ion evaporation from ion current measurements.

In contrast, the much smaller electrical conductivity of non-metallic liquids often has a large effect on the sharpness of the tip of the Taylor cones these liquids can form. The meniscus is no longer an equipotential surface, which brings in important influences of the liquid properties and flow rate on the maximum electric field E_{max} (Fernandez de la Mora & Loscertales 1994; Gañán-Calvo, *et al.* 1997; Higuera 2003*a*, and § 2 below). As a result, by controlling the liquid conductivity or the flow rate it is possible to shift from pure drop emission (the so-called colloidal regime), to a mixed mode including drops and ions (Gamero-Castaño & Fernandez de la Mora 2000*b*; Gamero-Castaño & Hruby 2001), and even to a purely ionic regime in the case of certain molten salts (Romero-Sanz *et al.* 2003; Romero-Sanz & Fernandez de la Mora 2004; Lozano 2003; Lozano & Martinez-Sanchez 2005). Ideally, the ion evaporation kinetics could be ascertained if the surface electric field and the ion current were simultaneously measured. Since the electric field at the surface is not directly measurable, we adopt here a mixed experimental/numerical procedure. The currents and flow rates of different solutions of ionic liquids are measured, and the surface electric field is computed as a function of the flow rate. Our computations will not include the effect of ion evaporation. Nevertheless, they can be used to derive information on the kinetics of ion evaporation when applied in the vicinity of the ion evaporation onset, where the ion current is small and its effect on the cone–jet can be neglected.

Although the literature on electrosprays (generally for mass spectrometric applications at atmospheric pressure, Fenn *et al.* 1989) is vast, here we shall be concerned only with the small fraction of such studies involving ion-evaporating Taylor cones formed in vacuo. There is a considerable body of work available based on glycerol, the mass spectrometer ramifications of which have been previously reviewed by Cook (1986), and the electrical propulsion applications of which have led also to a substantial literature (Perel *et al.* 1969; Huberman 1970; Huberman & Rosen 1974). That work has shown that glycerol cannot attain the high electrical conductivity necessary to evaporate ions from a single Taylor cone–jet, requiring instead a high-voltage rim emission mode. This result places glycerol beyond the limits of our analysis here, because our strategy depends on computing the electric field on the liquid surface. This is possible at present only for the regimes of Taylor cones that are well understood, which include single steady cone–jets but do not include the high-voltage rim emission mode.

Earlier attempts of Gamero-Castaño & Fernandez de la Mora (2000*a*) at inferring ion evaporating kinetics via ion current measurement from electrosprays of formamide electrolytes in vacuo were only partially successful due to several practical reasons. First, formamide has a non-negligible vapour pressure at room temperature. As a result, although its Taylor cones can be easily formed under vacuum, a fair fraction of the liquid flow rate injected upstream (up to 50 % in Gamero-Castaño & Hruby 2001) departs from the cone as vapour rather than as drops. This complicates the modelling of the meniscus behaviour, and creates ambiguities even in the jet flow rate and the local electrical conductivity at the emission region. Second, formamide sprays do carry a small component of ions, even under conditions when the field at the meniscus surface is unable to produce them. These ions appear to originate in the drops rather than the meniscus, so one has to deal with the complexity of distinguishing ions of two kinds.

Taylor cones of sulphuric acid held in a vacuum have been known for a long time to be a great source of ions (Perel *et al.* 1969). Surprisingly this interesting observation

γ (dyn cm^{-1})	$T_{boiling}$ (°C)	$T_{freezing}$ (°C)	p_v (55 °C) (Torr)	μ (20 °C) (g s^{-1} cm^{-1})	ρ (20 °C) (g cm^{-3})	ϵ (25 °C) —
41.93	241.7	−54.53	1.2	0.0276	1.2	64.92

TABLE 1. Some physical properties of propylene carbonate, from Riddick *et al.* (1986).

has not been followed up since. We have not pursued this option, in part due to the corrosive nature of this acid, and partly also because it is in this case difficult to reduce its electrical conductivity sufficiently to obtain a purely colloidal regime (drop emission only, no ions). Even if this were possible with suitable additives, for reasons to be discussed in the next paragraph, this relatively viscous liquid is even more prone than formamide to eject ions from the drops, precluding a clear study of the transition from the pure drop to the pure ion regime. The same difficulty presents itself in the case of molten salts, which tend to produce abundant drops as well as ions (Gamero-Castaño & Hruby 2001; Romero-Sanz, Aguirre-de-Carcer & Fernandez de la Mora 2005). And for those ionic substances that exceptionally yield only ions, no control parameter is available to enable a smooth transition from the purely colloidal to the purely ionic regime, very much as in the case of liquid metals.

Besides formamide electrolytes and molten salts or acids, no other non-metallic substances have been known to be able to eject ions from individual Taylor cones held in the cone–jet regime. However, while involved in electrical propulsion studies, we have found that certain electrolytes of the high-boiling-point solvent propylene carbonate (PC) evolve continuously from the purely colloidal regime (with no measurable ion evaporation from either the drops or the meniscus) to almost the purely ionic regime as one changes the liquid flow rate from high to low values. This singular situation is probably due to the smaller room temperature viscosity coefficient of PC (0.0276 g s^{-1} cm^{-1}) versus formamide (0.0376 g s^{-1} cm^{-1}). The effect of the liquid viscosity can be explained noticing that (i) on the reasonable assumption that the drop breakup time is short compared to the charge relaxation time, each primary drop will carry the electric charge that was present in the stretch of the jet from which the drop is formed, and (ii) the capillary instability leading to jet breakup produces larger drop/jet diameter ratios for more viscous fluids. This implies that the total charge of a drop, the charge per unit surface of the drop, and the ratio of the surface electric field at the larger drops to the maximum field at the jet, all increase with increasing viscosity for a given jet diameter (Gamero-Castaño & Fernandez de la Mora 2000*a*). A high viscosity thus favours ion evaporation from the drops, which is undesirable for our purposes here. This makes PC solutions more convenient than formamide. In addition, PC has a boiling point (241.7 °C) considerably higher than formamide (210.5 °C), giving hope (not fully materialized in the end) of a reduced volatility problem. These advantages of PC solutions have motivated the present effort to infer ion evaporation kinetics from measurements of ion currents versus liquid flow rate in these liquids. We exploit here the fact that, as well-known scaling arguments suggest (Fernandez de la Mora & Loscertales 1994; Gañán-Calvo *et al.* 1997; Higuera 2003*a*) and the computations of § 2 confirm, the electric field on the liquid surface is a well-defined decreasing function of the flow rate.

Some key properties of propylene carbonate are listed in table 1, where γ is the surface tension, μ is the viscosity coefficient, $p_v(T)$ is the equilibrium vapour pressure at temperature T, ϵ is the dielectric constant, and ρ is the density at 20 °C. PC

% (vol)	0.5	1	2	3.5	5	7.5	10	15	20	33	50
EMI-BF_4	0.102	0.22	0.38	0.45	0.66	0.97	1.04		1.59	1.87	2.02
EMI-Im					0.36	0.58		0.64	0.90	1.1	

TABLE 2. Electrical conductivities K (S/m) of the PC+ionic liquid mixtures investigated.

has a dielectric constant $\epsilon = 65$ ($\epsilon = 111$ in formamide; Riddick, Bunger & Sakano 1986). When mixed with ordinary salts, PC is inferior to formamide in terms of the electrical conductivities it can attain. While formamide electrolytes exceed room temperature conductivity values of $2\,\mathrm{S\,m^{-1}}$ with many inorganic salts (Bocanegra *et al.* 2004), PC reaches the $1\,\mathrm{S\,m^{-1}}$ level only in rare combinations. However, PC is freely miscible with a number of room-temperature molten salts, often referred to as ionic liquids (McEwen *et al.* 1999). Some of these mixtures are considerably less viscous and more electrically conducting than the neat ionic liquids. Consequently the present exploration will be based on combinations of PC with the two ionic liquids 1-ethyl-3-methylimidazolium bis(trifluoromethyl-sulfonyl)imide (EMI-Im) and 1-ethyl-3-methylimidazolium tetrafluoroborate (EMI-BF_4), with compositions and room-temperature electrical conductivities listed in table 2.

2. Computation of the electric field on the meniscus surface

Neither the electric field distribution along the meniscus surface, nor its maximum normal component, E_{max}, are measurable at present. Yet the electric field at the liquid surface is the main parameter governing ion evaporation kinetics, and must therefore be known to enable interpreting ion current measurements. In this section, the electric field distribution will be inferred from numerical calculations based on the work of Higuera (2003*a*) for a liquid with the physical properties of PC in the absence of ion evaporation. These results will then be used to analyse incipient ion evaporation. The computations of this section do not presuppose any scaling law. They simply assume that the liquid is a leaky dielectric (Saville 1997) with a spatially uniform electrical conductivity equal to that of the liquid injected upstream. The incompressible Navier–Stokes equations are solved for the liquid, coupled with Laplace's equation for the electric potential, and a transport equation for the surface charge. In order to circumvent the stiffness of the numerical problem, the equations are solved only in the transition region where the surface of the liquid departs from a Taylor cone and becomes a jet. Boundary conditions are obtained by matching with known asymptotic solutions in the cone and jet regions.

2.1. *Cone-to-jet transition region in the absence of ion evaporation*

The region of interest is sketched in figure 1. A constant flow rate of liquid Q is injected through the meniscus at the left side of the figure and pulled into the jet at the right side by the electric shear acting on the surface of the liquid. The surface is stationary and axisymmetric. It is subject to the pressure and viscous stresses of the liquid, $p\boldsymbol{n} - \boldsymbol{\tau}' \cdot \boldsymbol{n}$, to the surface tension stress $-\gamma C\boldsymbol{n}$, and to the electric stress, with components

$$\tau_n^e = \frac{\epsilon_0}{2}\left(E_n^2 - \epsilon E_n^{i^2}\right) + \frac{\epsilon_0}{2}(\epsilon - 1)E_t^2 \quad \text{and} \quad \tau_t^e = \sigma E_t \tag{2.1}$$

normal and tangent to the surface (Landau & Lifshitz 1960; Saville 1997). Here $\boldsymbol{n}$ and $\boldsymbol{t}$ are unit vectors normal and tangent to the surface and $C = \nabla \cdot \boldsymbol{n}$ is twice the

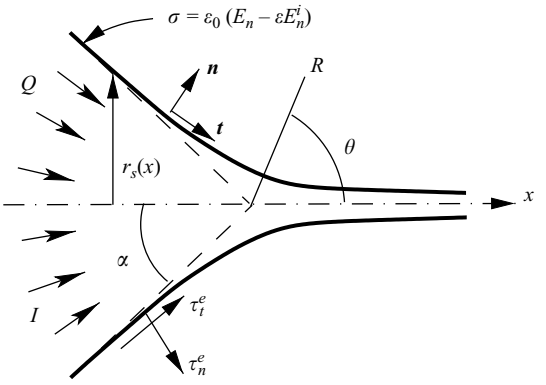

FIGURE 1. Sketch of the cone-to-jet transition region.

mean curvature of the surface; $\boldsymbol{\tau}'$ is the viscous stress tensor of the liquid and γ is its surface tension; ϵ_0 is the permittivity of vacuum; σ is the density of free charge at the surface of the liquid; and $\boldsymbol{E}$ and $\boldsymbol{E}^i$, with components (E_n, E_t) and (E_n^i, E_t^i) normal and tangent to the surface, are the electric fields in the vacuum and in the liquid. These fields are of the form $\boldsymbol{E} = -\nabla\varphi$ and $\boldsymbol{E}^i = -\nabla\varphi^i$, where, in the absence of space charge, the electric potentials φ and φ^i satisfy Laplace's equations in the vacuum and in the liquid. The conditions $\epsilon_0(E_n - \epsilon E_n^i) = \sigma$ and $E_t = E_t^i$ must be satisfied at the surface (Landau & Lifshitz 1960).

The electric field in the liquid induces a density of conduction current $\boldsymbol{j} = K\boldsymbol{E}^i$, where K is the electrical conductivity of the liquid. The component of $\boldsymbol{j}$ normal to the surface of the liquid accumulates electric charge at the surface, and this charge is convected by the flow, leading to a convection current I_s that adds to the axial conduction current in the bulk of the liquid I_b. In the absence of ion evaporation, the total current $I = I_b + I_s$ is a constant to be determined as part of the solution. The conduction current dominates in the conical meniscus, where the cross-section is large and the density of surface charge is small, and the convection current dominates in the jet, where the opposite conditions hold. In what follows, x and r are distances along and normal to the symmetry axis measured from the apparent apex of the Taylor cone, and R and θ are spherical coordinates (see figure 1). The surface of the liquid is sought in the form $r = r_s(x)$. The governing equations are

$$\nabla\cdot\boldsymbol{v} = 0, \quad \rho\boldsymbol{v}\cdot\nabla\boldsymbol{v} = -\nabla p + \mu\nabla^2\boldsymbol{v}, \quad \nabla^2\varphi^i = 0 \tag{2.2}$$

in the liquid, for $r < r_s(x)$,

$$\nabla^2\varphi = 0 \tag{2.3}$$

in the vacuum, for $r > r_s(x)$,

$$\gamma\nabla\cdot\boldsymbol{n} = p - \boldsymbol{n}\cdot\boldsymbol{\tau}'\cdot\boldsymbol{n} + \frac{\epsilon_0}{2}\left(E_n^2 - \epsilon E_n^{i^2}\right) + \frac{\epsilon_0}{2}(\epsilon - 1)E_t^2, \tag{2.4}$$

$$\boldsymbol{t}\cdot\boldsymbol{\tau}'\cdot\boldsymbol{n} = \sigma E_t, \tag{2.5}$$

$$\frac{\mathrm{d}}{\mathrm{d}x}(r_s v_s \sigma) = K r_s E_n^i\left(1 + r_s'^2\right)^{1/2}, \tag{2.6}$$

$$\sigma = \epsilon_0(E_n - \epsilon E_n^i), \quad E_t = E_t^i, \quad \boldsymbol{v}\cdot\boldsymbol{n} = 0 \tag{2.7}$$

at the liquid surface, $r = r_s(x)$; and the far-field ($R \to \infty$) boundary conditions

$$\varphi = -A\left(\frac{\gamma R}{\epsilon_0}\right)^{1/2} P_{1/2}(\cos\theta) + O\left(\frac{\rho^{1/2} Q^{1/2} I^{1/2}}{\epsilon_0^{3/4}\gamma^{1/4} R^{1/4}}\right) \tag{2.8}$$

in the vacuum, and

$$\varphi^i = -\frac{I}{2\pi(1-\cos\alpha)KR}, \tag{2.9}$$

$$\psi = -\frac{A\,P'_{1/2}(-\cos\alpha)}{2\pi(1-\cos\alpha)}\frac{\epsilon_0^{1/2}\gamma^{1/2} I}{\mu K} R^{1/2} f_B(-\cos\theta) + \frac{Q}{2\pi}\frac{1+\cos\theta}{1-\cos\alpha} \tag{2.10}$$

in the liquid.

Here ρ and μ are the density and viscosity of the liquid. Equations (2.4) and (2.5) are the balances of stresses normal and tangent to the surface, (2.6) is the transport equation for the surface charge, and (2.7) expresses the electrostatic conditions mentioned above and the condition that the liquid surface is a material surface in the absence of evaporation.

The first term on the right of the far-field boundary condition (2.8) for the electric potential in the vacuum is the electric potential of a Taylor cone (Taylor 1964). Here $P_{1/2}$ is the Legendre function of degree 1/2, $A = 2^{1/2}/[P'_{1/2}(-\cos\alpha)\sin\alpha\tan^{1/2}\alpha] \approx 1.3459$, and $\alpha = 49.29^\circ$ is the semiangle of a Taylor cone, which is the first zero of $P_{1/2}(\cos(\pi-\alpha))$. The second term on the right-hand side of (2.8) is the correction to Taylor's electric potential due to the electric charge of the jet (see Higuera 2003*a* for details). The electric potential (2.9) in the liquid far upstream of the apparent apex leads to the radial electric field needed to drive the current I. Since φ^i in (2.9) tends to zero faster than the two terms of (2.8) when $R \to \infty$, the condition $\varphi \approx 0$ must be satisfied at the surface of the meniscus in this far region. The surface may be sought here in the form $\theta = \pi - \alpha - \delta_s(R)$, where $\delta_s(R)$ is the departure of the surface from a Taylor cone. Applying this to (2.8) and setting $\varphi = 0$ gives $\delta_s(R) = O[(\rho Q I)^{1/2}/(\epsilon_0\gamma^3 R^3)^{1/4}]$ for $R \to \infty$.

Equation (2.10) gives the stream function of the flow in the liquid far upstream of the apparent apex. The last term of this equation is the sink flow due to the injected flow rate. The first term is the recirculating flow induced in the meniscus by the electric shear. The function $f_B(\xi)$, introduced by Barrero *et al.* (1999), is the solution of

$$\left.\begin{aligned} (1-\xi^2)\left(f_B^{iv} - 4\xi f_B''' + \frac{3}{2}f_B''\right) - \frac{15}{16}f_B = 0, \\ f_B(1) = f_B(\cos\alpha) = f_B''(\cos\alpha) + 1 = 0, \quad f_B'(1) < \infty. \end{aligned}\right\} \tag{2.11}$$

Characteristic values of the size R_c of the cone-to-jet transition region and of the flow variables (Q_c, E_c, I_c) in this region can be estimated from the following order-of-magnitude conditions: (i) The pressure variation induced by the flow should be of the order of the surface tension and normal electric stress in order for the surface to depart from a Taylor cone. Assuming that the inertia of the liquid plays a role (see Higuera 2003*a* for the case of a viscosity-dominated flow), the characteristic pressure variation is $p_c \sim \rho v_c^2$ with $v_c \sim Q_c/R_c^2$, and the condition reads $\rho Q_c^2/R_c^4 \sim \gamma/R_c \sim \epsilon_0 E_c^2$. (ii) The residence time of the flow in the transition region, $t_r = R_c/v_c$, should be of the order of the electric relaxation time, $t_e = \epsilon_0\epsilon/K$. The electric relaxation time is the time required by electric conduction normal to the surface to build up enough surface charge to affect the first boundary condition (2.7), i.e. $\sigma_c/t_e \sim \boldsymbol{j}\cdot\boldsymbol{n}$, with $\sigma_c \sim \epsilon_0 E_c \sim \epsilon_0\epsilon E_c^i$ and $\boldsymbol{j}\cdot\boldsymbol{n} \sim K E_c^i$, where σ_c and E_c^i denote the characteristic values

of the surface charge density and the electric field in the liquid. The surface charge would reach equilibrium and screen the liquid from the outer field ($\sigma \approx \epsilon_0 E_n \gg \epsilon_0 \epsilon E_n^i$ in (2.7)) if $t_r \gg t_e$, which seems to be the case for electrosprays operated at high flow rates. The condition $t_r \sim t_e$ was introduced by Fernandez de la Mora & Loscertales (1994) and defines the range of lowest flow rates at which a cone–jet can exist, which is the range of interest for ion evaporation (see also the comments at the end of this subsection). The bulk conduction current ($I_b \sim K E_c^i R_c^2$) and the surface convection current ($I_s \sim \sigma_c v_c R_c$) can be seen to be of the same order in the transition region when the condition $t_r \sim t_e$ is satisfied. Conditions (i) and (ii) taken together imply $R_c = \epsilon^{2/3} R_0$, $Q_c = \epsilon Q_0$, $E_c = E_0/\epsilon^{1/3}$, and $I_b \sim I_s \sim I_0$, where

$$R_0 = \left(\frac{\epsilon_0^2 \gamma}{\rho K^2}\right)^{1/3}, \quad Q_0 = \frac{\epsilon_0 \gamma}{\rho K}, \quad E_0 = \left(\frac{\gamma^2 K^2 \rho}{\epsilon_0^5}\right)^{1/6}, \quad I_0 = \frac{\gamma \epsilon_0^{1/2}}{\rho^{1/2}}. \tag{2.12}$$

If these factors are used to non-dimensionalize the problem (2.2)–(2.10), then the solution can be seen to depend only on the three dimensionless parameters ϵ, Re and Q/Q_0, where

$$Re = \frac{\rho Q_0}{\mu R_0} = \frac{\epsilon_0^{1/3} \rho^{1/3} \gamma^{2/3}}{\mu K^{1/3}} \tag{2.13}$$

measures the conductivity of the liquid. Numerical solutions of the dimensionless form of (2.2)–(2.10) have been computed for $\epsilon = 64.92$, $Re = 0.1$ and 0.2, and various values of Q/Q_0. The values $Re = 0.1$ and 0.2 are attained for PC at $K = 0.888$ S m^{-1} and 0.111 S m^{-1}, respectively.

The simplification brought about by confining the numerical computations to the transition region and using the far-field matching conditions (2.8)–(2.10) should be stressed. Computational studies of the breakup of a meniscus and the formation of drops in an electric field have been carried out by Notz & Basaran (1999) and Reznik *et al.* (2004) in the limits of negligible and dominant viscous effects, respectively. Both works solve the problem in the whole meniscus, but this is hardly feasible here because the ratio of the size of the meniscus to the radius of the jet may be above 1000 in typical cases. Furthermore, both works assume that the liquid is a perfect electric conductor and therefore the surface of the meniscus is an equipotential, while it is the breakdown of this assumption, as expressed by the condition $t_r \sim t_e$, which defines the transition region discussed here. The size of the transition region decreases when the conductivity of the liquid increases (see (2.12) above and Fernandez de la Mora & Loscertales 1994; Gañán-Calvo, *et al.* 1997; Higuera 2003*a*), but the region always plays a key role in determining the electric current and the radius of the jet in the conditions under scrutiny. The limit of infinitely large electrical conductivity is a singular limit for our problem, and the surface is never an equipotential.

Table 3 collects results from the computations for two different electrical conductivities and the dimensionless flow rates indicated in the first column. The largest values of Q/Q_0 for which converged solutions have been obtained are somewhat smaller than the typical experimental values found for this parameter, so that the most physically relevant data are those at the bottom of the two data sets tabulated. Experience with these computations suggests that the convergence limitations at high flow rates depend on the iterative scheme used in our code rather than on the physics of the problem.

The second column of table 3 gives the dimensionless electric current. In the third and fourth columns E_{max} and $r_{s_{max}}$ stand for the maximum value of E_n on the surface and the radius of the jet at the position of this maximum. These variables are scaled

$\frac{Q}{Q_0}$	$\frac{I}{I_0}$	$\frac{E_{max}}{E_k}$	$\frac{r_{s_{max}}}{R^*}$	$\frac{I/I_0}{(Q/Q_0)^{1/2}}$	$-\left(\frac{\mathrm{d}^2(E/E_k)}{\mathrm{d}(x/R^*)^2}\right)_m$	$-\left(\frac{\mathrm{d}r_s}{\mathrm{d}x}\right)_m$	δ
			$K = 0.111$ S m^{-1} ($Re = 0.2$)				
0.818	0.998	0.70886	0.879	1.10345	0.00721	0.04463	150.125
2.306	1.808	0.73103	0.942	1.19061	0.00658	0.04630	175.088
4.697	2.758	0.7467	0.986	1.27258	0.00577	0.04636	200.848
5.392	2.987	0.75083	0.998	1.28635	0.00546	0.04649	210.549
5.509	3.025	0.75219	0.994	1.28881	0.00543	0.04656	210.741
5.754	3.103	0.74964	0.996	1.29359	0.00533	0.04639	212.211
6.639	3.374	0.74442	1.014	1.30947	0.00513	0.04568	218.224
			$K = 0.888$ S m^{-1} ($Re = 0.1$)				
0.312	0.652	0.73379	0.900	1.16727	0.01985	0.00752	157.232
0.729	1.038	0.76179	0.925	1.21572	0.00912	0.00701	175.442
0.759	1.06	0.75833	0.932	1.2167	0.00891	0.00708	174.710
6.782	3.71	0.77871	1.079	1.42461	0.00081	0.00399	278.475
8.941	4.329	0.77364	1.115	1.44775	0.00058	0.00360	300.757

TABLE 3. Computational results for room-temperature PC.

with the electric field variable E_k of Gamero-Castaño & Fernandez de la Mora (2000*a*) and the length variable R^* of Fernandez de la Mora & Loscertales (1994), which are given by

$$E_k = \frac{\gamma^{1/2} K^{1/6}}{\epsilon_0^{2/3} Q^{1/6}} \quad \text{and} \quad R^* = \left(\frac{\epsilon_0 Q}{K}\right)^{1/3}, \tag{2.14}$$

so that $E_{max}/E_k = (E_{max}/E_0)(Q/Q_0)^{1/6}$ and $r_{s_{max}}/R^* = (r_{s_{max}}/R_0)/(Q/Q_0)^{1/3}$ in terms of the dimensionless variables based on (2.12).

Of particular interest is the fact that, although E_{max}/E_k varies by a few percent from the largest to the smallest flow rates shown, it is essentially independent of Q when one excludes the physically dubious values of Q/Q_0 below 4. This confirms as an excellent approximation the scaling $E_{max} \sim E_k$ of Gamero-Castaño & Fernandez de la Mora (2000*a*) for the flow rate dependence. One sees a 5 % variation in E_{max}/E_k upon increasing the electrical conductivity by a factor of 8. This invalidates slightly the K dependence involved in the assumption $E_{max} \sim E_k$, though still shows it to be an excellent approximation over the whole range of numerical (and experimental) conditions explored. Similar considerations apply to $r_{s_{max}}/R^*$. For all practical purposes, with a maximum global error of about 2 %, we can therefore describe these numerical computations through

$$E_{max} = \beta E_k \quad \text{with} \quad \beta \approx 0.76 \qquad \text{and} \qquad r_{s_{max}} \approx R^*. \tag{2.15}$$

Numerical computations carried out by Carretero (2005) with a different model and numerical method confirm the scaling law $E_{max} \sim E_k$. This author finds $\beta \approx 0.79$ for octanol ($\epsilon = 10.34$) and $\beta = 0.96$–1.13 for formamide ($\epsilon = 111$) in different ranges of conductivity and flow rate. These results suggest a monotonic increase of β with ϵ and a value of β for PC ($\epsilon = 64.92$) slightly larger than that in (2.15).

The fifth column in table 3 represents the ratio $I/(\gamma K Q)^{1/2}$, which according to the measurements of Fernandez de la Mora & Loscertales (1994) should take a value of about 2.2 for a liquid with the dielectric constant of PC. The calculations show a considerably smaller value (1.3–1.4), which is furthermore dependent on flow rate. We

note however, that the measurements quoted did not include PC, did only show an approximate $I \sim (\gamma K Q)^{1/2}$ dependence, and were in addition taken at considerably smaller electrical conductivities and dimensionless flow rates substantially larger than those used in the present computations.

The solution discussed here for the small cone-to-jet transition region is largely independent of how the rest of the meniscus is set up. It only requires: (i) that the electric field tend to the field computed by Taylor (1964) for a conical meniscus (slightly modified by the presence of the jet) when $R \to \infty$, see (2.8); and (ii) that the flow rate to be ejected by the jet (Q in (2.10)) be specified. In the operation of an electrospray, the first condition is satisfied when the transition region is preceded by a large nearly hydrostatic region, because the balance of electric and surface tension stresses renders the meniscus conical in the hydrostatic region. But it is not easy to set the flow rate entering the transition region to an arbitrarily small value, because the rest of the meniscus acts as a large reservoir from which the transition region can draw a flow rate larger than the flow rate fed through the capillary. When this happens, the meniscus is slowly depleted until an equilibrium is reached or the formation of a cone ceases to be possible and the jet stops. The order-of-magnitude estimates discussed above (see also Fernandez de la Mora & Loscertales 1994; Higuera 2003*a*) show that the electric shear stress acting on the surface of the liquid in the transition region can draw a flow rate of order ϵQ_0 from the conical meniscus, and therefore it would be difficult to operate an electrospray steadily at flow rates much smaller than this value. The estimate ϵQ_0 is in line with experimental results for the minimum flow rate at which a cone–jet can be established. The limitation, however, does not come from the transition region itself, which may explain why the computations of this section yield stationary solutions even at flow rates smaller than the experimental minimum.

2.2. *Incipient ion evaporation*

The ion evaporation theory of Iribarne & Thomson (1976) gives the ion current evaporated per unit area of the surface (j_i) as the following function of the local electric field on the vacuum side of the liquid surface (E):

$$j_i(E) = \frac{kT}{h}\epsilon_0 E \exp\left[-\frac{\Delta G - G(E)}{kT}\right], \tag{2.16}$$

where T is the absolute temperature, k and h are Boltzmann's and Planck's constants, ΔG is the Gibbs free energy required to bring an ion (perhaps solvated) from the solvent into the vacuum, and $G(E)$ is the reduction in ΔG due to the presence of the electric field E. For a liquid of high dielectric constant and a surface with a radius of curvature of several nanometres, $G(E)$ may be written through the Schottky hump approximation (Loscertales & Fernandez de la Mora 1995) as

$$G(E) = \left(\frac{e^3 E}{4\pi\epsilon_0}\right)^{1/2}. \tag{2.17}$$

The total ion current is

$$I_i = \int 2\pi r_s \sqrt{1 + \left(\frac{\mathrm{d}r_s}{\mathrm{d}x}\right)^2}\, j_i(E)\,\mathrm{d}x. \tag{2.18}$$

The value of $\Delta G/kT$ is expected to be large at room temperature, at which the rate of ion evaporation (2.16) is exponentially small in the absence of an electric field and very sensitively dependent on the value of the field at the surface. The quantity $G(E_{max})/kT$ must also be large for ion evaporation to have any effect; $G(E_{max}) = \Delta G$ can serve as a rough definition of an evaporation onset.

Intense ion evaporation leads to a space charge around the liquid, which should be taken into account by modifying (2.3), and to an electric current and a mass flux across the liquid surface, which should be included in (2.6) and the third boundary condition (2.7). However, all these effects are small near the onset of evaporation or below, and then the numerical solution of (2.2)–(2.10) can be used to compute the ion current (2.18) with good approximation. In these conditions of incipient evaporation j_i has a sharp maximum at the point of the surface where the electric field is maximum and falls abruptly away from this point. The Laplace method can therefore be used to simplify the computation of the integral in (2.18) by approximating $E(x)$ in the exponent of (2.16) as a local parabola in the vicinity of its maximum and writing $G(E) \approx G(E_{max}) + (\mathrm{d}G/\mathrm{d}E)_{E_{max}}(E - E_{max}) = G(E_{max})(1 + \frac{1}{2}(E - E_{max})/E_{max})$. The result is

$$I_i = \delta \frac{kT}{h} \epsilon_0 E_k R^{*2} \left(\frac{kT}{G(E_k)} \right)^{1/2} \exp\left[-\frac{\Delta G - (E_{max}/E_k)^{1/2} G(E_k)}{kT} \right] \tag{2.19}$$

with

$$\delta = 4\pi^{3/2} \frac{r_{s_{max}}}{R^*} \sqrt{1 + \left(\frac{\mathrm{d}r_s}{\mathrm{d}x} \right)_m^2} \frac{(E_{max}/E_k)^{5/4}}{\left[-\mathrm{d}^2(E/E_k)/\mathrm{d}(x/R^*)_m^2 \right]^{1/2}}. \tag{2.20}$$

Here the subscript m means conditions at the point of the surface where the normal field attains its maximum E_{max}, and use has been made of the definitions (2.14).

The values of δ computed from the solution of (2.2)–(2.10) are given in the last column of table 3. This quantity turns out to be considerably larger than unity and to increase with the dimensionless flow rate Q/Q_0, which is due to the fact that the second derivative term in the denominator of (2.20) is very small and decreases slightly with increasing Q/Q_0. The small value of $[-\mathrm{d}^2(E/E_k)/\mathrm{d}(x/R^*)^2]_m$ (sixth column of table 3) reveals that R^* in (2.14) is not an accurate estimate of the size of the region of high surface field, which extends to distances around the position of maximum field large compared to the radius of the jet $r_{s_{max}}$. For all the conditions of table 3, δ spans the range from 150 to 300.

The result (2.19) is a refinement of the original estimate of Gamero-Castaño & Fernandez de la Mora (2000*a*), who approximated $(kT/G(E_k))^{1/2}\delta$ as a constant of order unity.

3. Experimental

The experimental system is sketched in figure 2, and is based closely on those previously used by Gamero-Castaño & Hruby (2001), Bocanegra *et al.* (2004), Romero-Sanz *et al.* (2003), and Romero-Sanz & Fernandez de la Mora (2004). The electrolyte to be electrosprayed is held inside a polypropylene vial sealed with an o-ring cap (top left, labelled 'liquid deposit'). A silica capillary (20 μm ID, 360 μm OD; Polymicro Technologies) has one end inside the liquid in the vial, another inside a vacuum chamber, and enters both in a leak free fashion through a pair of liquid chromatography connectors (Upchurch Scientific). The pressure ΔP inside the polypropylene vial can be varied from a fraction of a torr to several atmospheres, and is used to control the flow rate at which the liquid is fed from the reservoir to the sharpened end of the capillary held inside the vacuum chamber. This emitter end is approximately conical with a tip diameter close to 20 μm. It is made conducting by depositing a thin film of tin oxide, kept in electrical contact with a metallic tube. This tube also centres the emitter tip with respect to an extractor electrode. The emitter

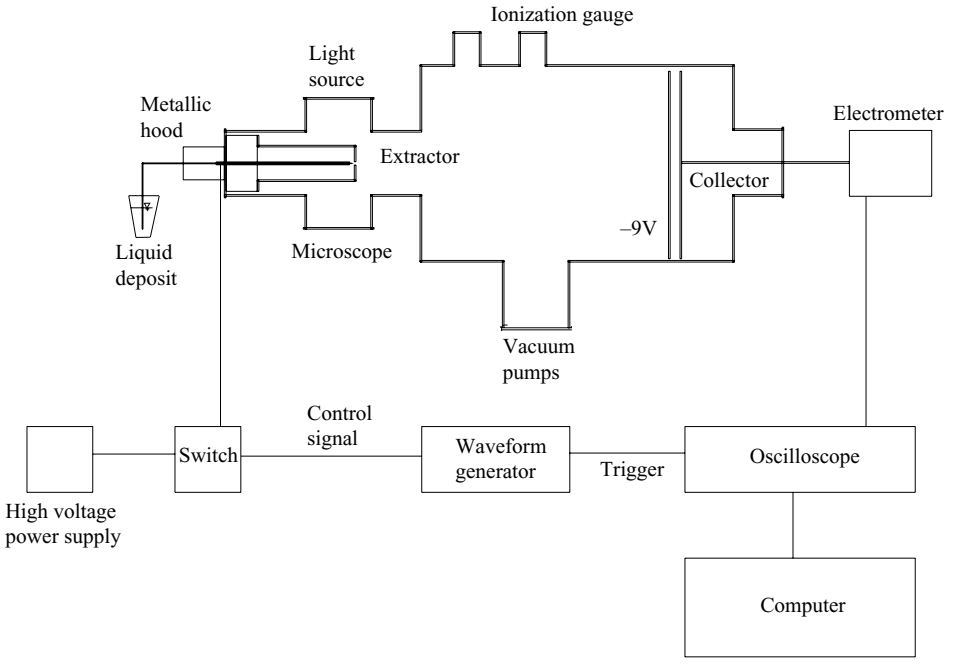

FIGURE 2. Sketch of the experimental setup.

is surrounded axisymmetrically by a cylindrical electrode (labelled 'extractor' in the figure), closed at its right end with a flat disk with a centred hole 2.5 mm in diameter. The drilled extractor disk is located 2 mm away from the emitter tip. It is connected to an electrometer used to establish that no spray current is collected in it, whereby all the spray passes through the hole, enters the vacuum chamber and freely flies axially towards a collector electrode. This collector is a flat metallic disk 27.8 cm in diameter, held normal to the axis of the emitter, and located 22.8 cm downstream from the extractor. The collector is virtually grounded through a fast ($\sim$0.1 μs rise time) electrometer, and is preceded a short distance upstream by a grid (held at -9 V) 90 % transparent to ensure that the arriving charged particles are not sensed by the collector prior to actually reaching it. The charge distribution of the sprays produced was studied by time-of-flight analysis, by suddenly grounding the emitting tip at time $t = 0$, and recording the current trace $i(t)$ received at the electrode in a digitizing oscilloscope (Gamero-Castaño & Hruby 2001). This $i(t)$ curve gives the velocity distribution of the particles produced, and permits a ready distinction between fast ions and slow drops. 1-ethyl-3-methylimidazolium tetrafluoroborate (EMI-BF_4) was purchased from Fluka, 1-ethyl-3-methylimidazolium bis(trifluoromethylsulfonyl)imide (EMI-Im) was from Covalent Associates, and propylene carbonate from Sigma Aldrich (99.7 % purity).

4. Experimental findings

4.1. *PC seeded with EMI-BF_4*

Figure 3 shows a series of time-of-flight (TOF) data obtained with the EMI-BF_4 mixtures. At time $t = 0$, just when the spray is interrupted, all the current is reaching the collector, and it eventually begins to diminish as the charged particles initially

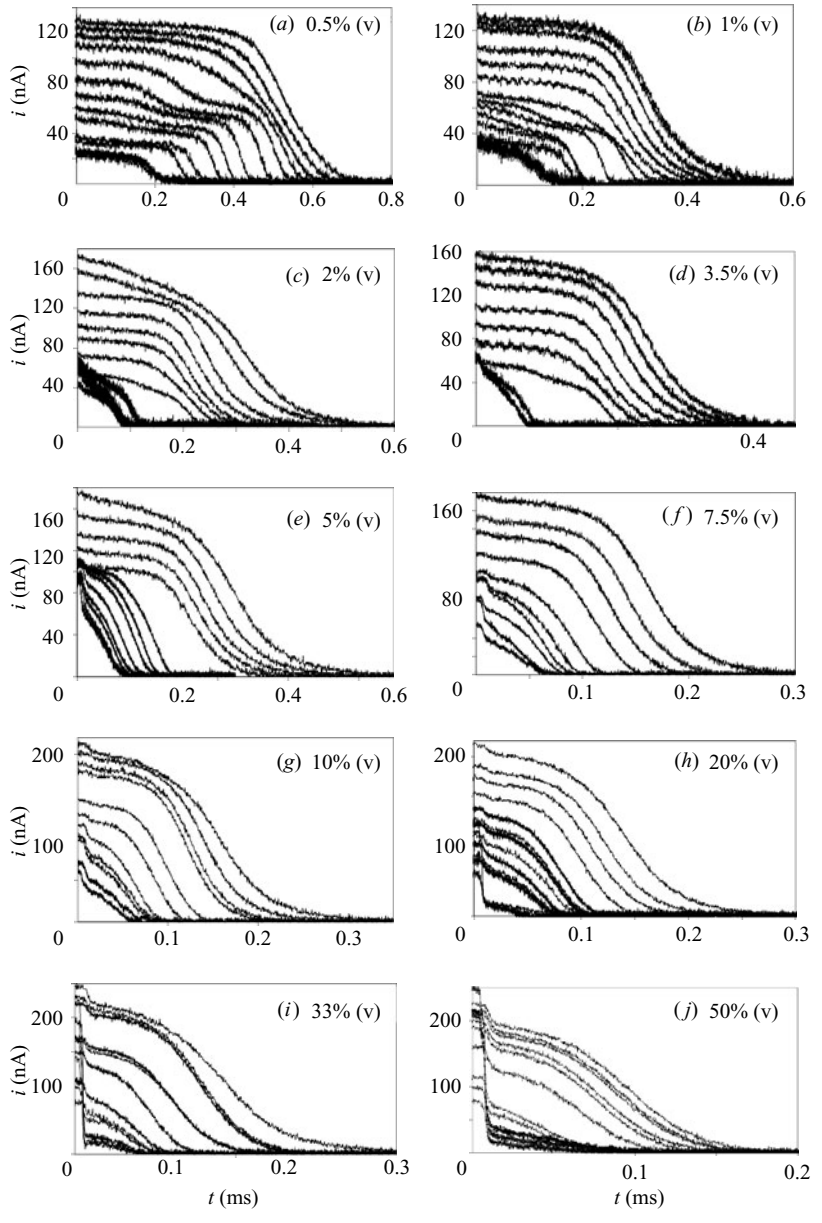

FIGURE 3. Time-of-flight distributions for sprays of PC with EMI-BF_4 at several concentrations and liquid flow rates. The curves give the electric current $i(t)$ reaching the collector as a function of time following the interruption of the spray at $t = 0$. Each curve is for a given flow rate, which increases from bottom to top in each panel.

contained in the space between the source and the collector are exhausted by flying into the collector, which happens first with the fastest particles. The flow rate of the spray is given by equation (5.1*a*) below in terms of the collected electric current $i(t)$ in figure 3, the voltage V_a accelerating the particles, and the distance L between extractor and collector in figure 2; see Gamero-Castaño & Hruby (2002) for details.

At the lowest salt concentration (0.5 % vol.) the pattern of figure 3 is similar to that previously reported for mixtures of tributyl phosphate with EMI-Im (Gamero-Castaño & Hruby 2002), with well-defined single steps at low flow rates, evolving first into double steps (main and satellite drops), and into a single broad step at high flow rates. This double step structure has been exploited previously to determine not only the charge over mass ratios, q/m for both drop types, but also (from energy measurement of both drop types) the voltage and velocity of the jet at the breakup point (Gamero-Castaño & Hruby 2002). At higher flow rates the curves exhibit a broader single step characteristic of a more disordered jet breakup mechanism. There is a similar tendency to form less sharp steps at increasing salt concentration. At about 2 % salt volume fraction, one begins to see a small step associated to ions with short flight times. In ordinary electrosprays (no ions) the current and the drop size depend little on needle voltage (Fernandez de la Mora & Loscertales 1994). This ceases to be the case once ion evaporation sets in, as seen in the two separate groups of curves shown in figures 3(*c*) to 3(*e*), where those further to the left correspond to higher needle voltages. The trend to produce ions is already quite substantial at the smallest flow rates for 5 % salt volume fraction, and becomes measurable even at high liquid flow rates at salt concentration above 10 % (vol). The tendency to produce more ions at lower flow rates and higher electrical conductivities is to be expected from the known fact that both these variables sharpen the apex region (cone–jet) of the meniscus (Fernandez de la Mora & Loscertales 1994; Rosell-Llompart & Fernandez de la Mora 1994). This yields higher local electric fields that reduce the activation barrier for ion evaporation (Iribarne & Thomson 1976; Loscertales & Fernandez de la Mora 1995). This trend is qualitatively similar to that previously observed with formamide-NaI solutions (Gamero-Castaño & Fernandez de la Mora 2000*b*; Gamero-Castaño & Hruby 2001; Bocanegra *et al.* 2004). However, there is a quantitative difference in that the onset of ion evaporation corresponds here to substantially lower electrical conductivities than in formamide-NaI solutions. One is tempted provisionally to interpret this difference as implying that the EMI^+ ion is more volatile (has lower solvation energy) than solvated Na^+, though the matter is by no means so simple (see § 4.4). The opposite effect of a large decrease in ion volatility has been observed in formamide upon trading the Na^+ for the less volatile NH_4^+ ion (Bocanegra *et al.* 2004).

The drop current in figure 3 (given by the height of the steps further to the right) decreases on reducing the liquid flow rate, while the ion current (given by the height of the step at short flight times in figures 3*c* to 3*j*) has the opposite behaviour. At all salt concentrations below 20 % (vol) studied (small electrical conductivities and large flow rates) the first effect is dominant, and the total current decreases monotonically with the liquid flow rate. Above 20 % salt concentration one observes a minimum in the current vs. flow rate curve, and the ion current dominates over the drop current at low enough flow rates. Again, with the quantitative differences noted, this is qualitatively similar to the behaviour previously found in formamide–NaI electrolytes. We have attempted to plot the ion current versus the electric field variable (2.14) but this has led to a poor correlation between data series with different electrical conductivities. The probable reason is that the substantial quantities of ionic liquid required to attain adequate electrical conductivities here modify other important liquid properties, particularly the viscosity. A note of caution is also necessary in relation to the data exhibiting dominant ionic currents at 33 % and 50 % salt. Because the liquid flow rates are very low in these cases, it is possible that evaporation of the solvent might have depleted its original concentration in the solution. As a confirmation of this suspicion,

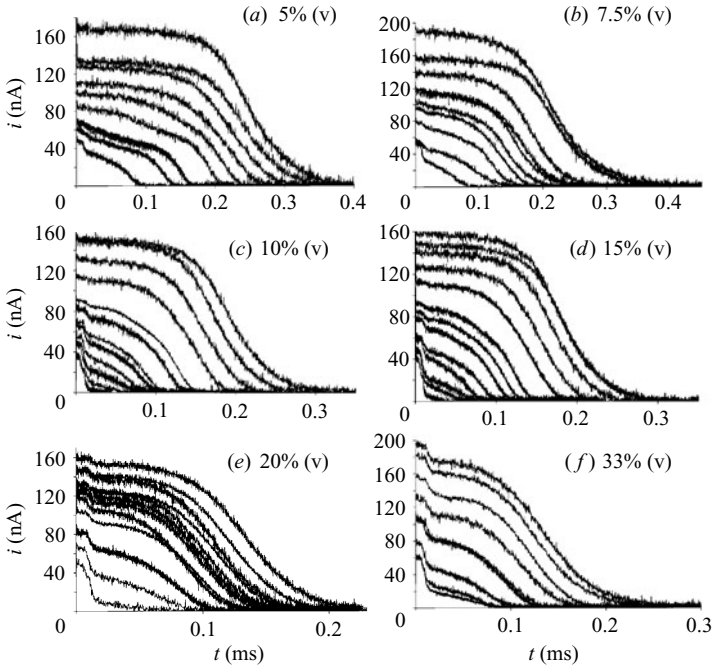

FIGURE 4. Time-of-flight distributions for sprays of PC with EMI-Im at several concentrations and liquid flow rates (increasing from bottom to top in each panel).

we note the fact that the needle tended to wet under such low flow rate conditions. As a result, a large drop developed near the meniscus, whose long residence time ensured that it was of pure ionic liquid (which is highly involatile). The emissions observed under these problematic conditions furthermore resemble very much those reported by Romero-Sanz *et al.* (2003) for pure EMI-BF_4, casting further doubts on their validity.

4.2. *PC seeded with EMI-Im*

PC/EMI-Im mixtures have been studied in less detail at small salt concentrations, with corresponding TOF curves shown in figure 4. The most striking differences with the previous data are:

(i) The total current always varies monotonically with liquid flow rate (no current maximum).

(ii) A continuous evolution from almost no ion production at high flow rates to almost no drop production at low flow rates is observed at 10 % and 15 % (vol) concentration of ionic liquid.

(iii) The almost purely ionic regime seen at 10 % and 15 % (vol) EMI-Im is approached not only via a gradual reduction of the drop current, but also by a simultaneous gradual reduction of the diameter of the emitted drops.

For unclear reasons, the PC/EMI-Im mixtures do not seem to suffer the same level of difficulty associated to solvent volatility and needle wetting noted for PC/EMI-BF_4. This is clear from the data in figure 4, as pure EMI-Im does not reach the ion-dominated regime at room temperature, while it almost does in two of the mixtures with PC. In addition, there is an excellent correlation between measured ion current and the electric field variable E_k defined in (2.14). Note, however, that the liquid flow rate Q ($m^3\,s^{-1}$) injected through the Taylor cone used to compute

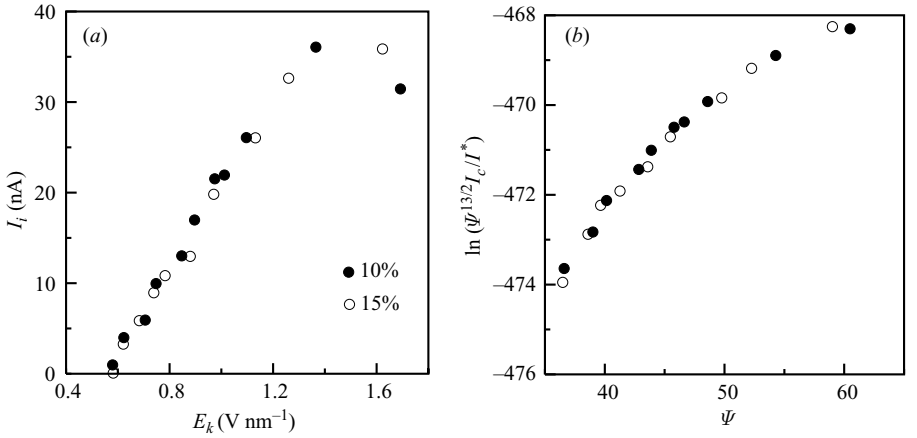

FIGURE 5. Ion current (nA) represented in terms of both (*a*) the electric field variable E_k of equation (2.14), and (*b*) as suggested by ion evaporation theory, where $kT\Psi$ is the reduction in the activation barrier expected from a surface electric field E_k, for two concentrations of EMI-Im/PC.

E_k was not directly measured, but is instead inferred from the TOF traces (see § 5). As shown in figure 5(*a*) for the 10 % and 15 % (vol) solutions, the ion current vs. E_k curves are almost identical for both solutions, with an onset of ion evaporation at about $E_k = 0.55$ V nm^{-1} ($E_{max} = 0.42$ V nm^{-1}). This field is considerably smaller than seen previously for formamide electrolytes, confirming more quantitatively our earlier observation of substantial ion evaporation from PC/EMI-Im electrolytes at unusually small electrical conductivities.

4.3. *Ion evaporation kinetics*

Let us define $\Psi = G(E_k)/kT$. Using (2.14) and (2.17), the pre-exponential factor in (2.19) can be rewritten as

$$\delta \frac{kT}{h} \epsilon_0 E_k R^{*2} \left(\frac{kT}{G(E_k)} \right)^{1/2} = \frac{I^*}{\Psi^{13/2}} \quad \text{with} \quad I^* = \frac{\delta e^9 \gamma^2}{(4\pi)^3 h (kT)^5 \epsilon_0^4}, \tag{4.1}$$

and (2.19) can be written more compactly as

$$\ln \left(\Psi^{13/2} \frac{I_i}{I^*} \right) = -\frac{\Delta G}{kT} + \beta^{1/2} \Psi, \tag{4.2}$$

with $\beta = E_{max}/E_k$ as defined in the first equation (2.15). Leaving out the mild dependence of δ on the flow rate (and thus on Ψ), it follows that the natural logarithm of the product $\Psi^{13/2} I_i/I^*$, when plotted versus the variable Ψ should yield a straight line with a slope $\beta^{1/2}$ in the regime of incipient ion evaporation. Such a plot is shown in figure 5(*b*) for the data from 10 % and 15 % EMI-Im in PC, with the constant value $\delta = 250$ used in the definition of I^*. The curve is not straight. But its curvature at high ion current is not surprising, as the arguments used to establish the maximum electric field as being proportional to E_k are based on the scaling laws for the cone–jet in the absence of ion evaporation. Equation (4.2) can therefore be expected to hold only when the ion current is small compared to the drop current, which is only a few tens of nA. Since our noise level in these data is about 1 nA, we are limited by the two conflicting requirements 1 nA $\ll I_i \ll$ 40 nA. An approximate slope can be determined in figure 5(*b*) by making use of the three

lowest data points, the highest of which correspond to ion and drop currents of 10 nA and 72 nA, respectively. In spite of the imprecision of this measurement, the slope is certainly smaller than 1/2, which would yield the unexpectedly small upper bound value $\beta_{exp} < 0.25$. The activation energy ΔG derived from these data is about 1.14 eV, which is anomalously low.

4.4. *Discussion*

The anomalous ΔG value obtained could be due to a number of causes, some of which are discussed below.

(i) The assumption that the ion current should be small compared to the drop current appears to be insufficient to ensure that ion evaporation is not affecting the flow and the transport of charge in the liquid. Since ion evaporation is a localized process on the surface of the liquid, a more appropriate condition could be that the maximum ion current density, $j_{i_{max}} = j_i(E_{max})$ given by (2.16), should be small compared to the density of conduction current reaching the surface from the bulk of the liquid at the position of E_{max}. The maximum ion current density is, from (2.19), $j_{i_{max}} = [G(E_k)/kT]^{1/2}(E_{max}/E_k)(I_i/R^*\delta)$, where I_i is the measured ion current. On the other hand, the conduction current density would be $j_{c_{max}} = K E_n^i = K E_{max}/\epsilon$ in the absence of surface charge (from the first boundary condition (2.7) with its left hand side set to zero), while the real conduction current density should be smaller than this value when the surface charge partially screens the liquid from the outer field. The ratio

$$\frac{j_{i_{max}}}{j_{c_{max}}} = \frac{\epsilon}{\delta}\left(\frac{G(E_k)}{kT}\right)^{1/2}\frac{I_i}{K E_k R^{*2}} \tag{4.3}$$

is not very small in our experiments. For example it is about 0.14 for 10 % EMI-Im in PC with $I_i = 4$ nA. This suggests that the measurements should be extended to still smaller levels of ion current, at which the assumption of negligible effects of ion evaporation on the cone–jet structure would be more rigorously met. An initial attempt in this direction was undertaken in Espina-Trigo (2004) through efforts to reduce the noise level of the ion current measurement. Her data show a trend towards more realistic values of β, and slightly larger ΔG, but the latter is still too low to be credible. Because she used the same experimental method as described here, the problem appeared to be that the improvement in ion current sensitivity was insufficient. Her findings stimulated an unpublished Senior Thesis by B. Jorns, based on a new technique to measure the current of ions. This is done by stopping them (but not the drops) in a finite background pressure, similarly to Gamero-Castaño & Fernandez de la Mora (2000*b*), with improvements due to V. Fasson (unpublished Senior Thesis). The ion current is now measured directly down to 0.01 nA, rather than by identifying a tiny step over a total electrospray current of tens or hundreds of nA. Provisional results from Jorns's study yield reasonable activation energies. In conclusion, theoretical results and preliminary experiments coincide in indicating that our measurements cannot be interpreted on the basis of the purely colloidal regime.

(ii) The alternative that ion evaporation theory is incorrect must be rejected in view of several prior studies based on the evolution of the charge on evaporating drops as a function of their radius. Although the drops evolve too fast to be directly examined, the salt clusters left after their complete evaporation remain as indicators of their final size and charge, and in all available studies these have confirmed ion evaporation theory with reasonable solvation energies of $\sim$1.8 eV, even for non-aqueous solvents (formamide) and for large and relatively volatile ions (Loscertales & Fernandez de

la Mora 1995; Gamero-Castaño & Fernandez de la Mora 2000*b*; Fernandez de la Mora, Thomson & Gamero-Castaño 2005; Ku & Fernandez de la Mora 2004).

(iii) We have considered as another alternative the possibility that ion evaporation from a drop differs considerably from ion evaporation from the cone–jet transition. Note in particular that the electric field here is not normal to the surface. It includes a substantial tangential component, particularly at the point where the maximum normal field is reached. A model conceptually equivalent to that underlying the Schottky hump (2.17) involves launching the ions with a certain initial direction and energy, and allowing them to evolve in the computed external field until they overcome the barrier associated with their own image force on the liquid. An optimal launching direction and a minimal initial energy can then be computed numerically, similarly to the Shottky model. Unfortunately, a limited level of analysis of this possibility indicates that the effect of the axial field is insufficient to reduce the activation energy by the required $\sim$0.7 eV.

Another possible weak point in the experimental procedure is associated with the finite vapour pressure of PC. We have noted a large boiling point difference between PC and formamide, but this must be tempered with the fact that formamide decomposes at this 'boiling point' (Ridick *et al.* 1986). The consequences of solvent evaporation are of two kinds. First, the preferential evaporation of the solvent in the meniscus increases the solute concentration, and therefore the electrical conductivity of the solution (particularly at the surface). Second, the flow rate Q_i of liquid injected through the capillary goes only partly into the jet, the balance being lost by evaporation from the meniscus surface. Q is therefore smaller than Q_i, with losses that have been reported to be up to 50 % in formamide electrolytes (Gamero-Castaño & Hruby 2001). In our case however, we do not measure Q_i, but infer Q directly from the TOF traces (§ 5).

That solvent evaporation from the meniscus is not negligible is qualitatively clear from the results already discussed with respect to concentrated PC/EMI-BF_4 mixtures. At least under some conditions, it was apparent that all the PC evaporated and the emissions were from the neat ionic liquid. In order to better quantify the magnitude of solvent evaporation from the meniscus, we have run several series of experiments comparing the current versus flow rate dependence of our Taylor cones both under vacuum and under atmospheric pressure. Given the high boiling point of PC (240 °C), evaporation under atmospheric conditions is negligible. These experiments were done in mixtures of PC seeded with EMI-BF_4 at volume concentrations of 0.5 % and 50 %. Owing to the greater importance of space charge effects under atmospheric conditions, the voltages used in both cases were adjusted to slightly different values, such as to obtain the same shape of Taylor cone. The flow rates were made identical in both cases by establishing the same pressure difference ΔP between the liquid reservoir and the emitting tip of the capillary. The results of these experiments are collected in table 4 in the form of the electrospray current under vacuum and atmospheric condition versus the flow rate variable ΔP. As can be seen, a substantially smaller current is recorded under vacuum. Under the assumption that $I \propto (KQ)^{1/2}$ this implies that the expected increase in K resulting from solvent evaporation is considerably smaller than the associated decrease in Q. Although a quantification of these observations is difficult, they certainly show qualitatively that solvent evaporation remains an issue. Future work should make use of capillary tip diameters considerably smaller than the 20 μm used here. On the other hand, notice that obtaining the expected activation energy requires substantial increases of E_k. Because $E_k \propto (K/Q)^{1/6}$, even doubling K and halving Q would be insufficient to correct the anomaly observed.

0.5 % (vol) PC/EMI-BF_4			50 % (vol) PC/EMI-BF_4		
ΔP (PSI)	I_{atm} (nA)	I_{vac} (nA)	ΔP (PSI)	I_{atm} (nA)	I_{vac} (nA)
15	210	170	15	380	210
10	170	150	10	350	340
5	140	130	5	330	270
0	150	110	0	300	300
−5	130	90	−5	370	300
−10	110	80	−10	200	240
−15	110	70			

TABLE 4. Electrospray current I in the atmosphere and under vacuum versus liquid flow rate (quantified through the pressure ΔP driving the liquid through the capillary).

A final potentially weak point deserving discussion is the constant-conductivity hypothesis used in the computational model. Fernandez de la Mora & Loscertales (1994) have argued that one factor determining the smallest possible flow rate at which a Taylor cone may be stabilized is set by the condition that all the incoming ions of one polarity but none of the opposite polarity be ejected with the jet. This sets a maximum value of the current $I_{max} = neQ$, where n is the positive (monovalent) ion concentration in the incoming flow and e is the elementary charge. The intersection of this $I_{max}(Q)$ curve with the real $I(Q)$ curve of the electrospray defines a lowest possible flow rate below which charge neutrality could not be maintained in the liquid. At this limit, the interior of the liquid jet cannot hold any charge, since no negative ions are available. All the positive charge would then be on the surface, and the bulk electrical conductivity of this liquid would be zero, rather than its upstream value. Although this situation may appear extreme, it is in fact encountered experimentally near the minimum flow rate in polar and low-viscosity liquids such as water and formamide. Presumably the same situation would be obtained for PC, so the leaky dielectric model cannot be correct near the minimum flow rate. In spite of this ambiguity, note that the smallest ion currents marking the ionization onset correspond to drops currents (∼100 nA) considerably larger than the minimum drop current, which can be safely inferred from the lower conductivity data (∼30 nA). Hence, the experimental data that define the onset value of E_k are sufficiently far from the minimum flow rate for the constant-conductivity hypothesis to be adequate.

In conclusion, we have considered the simplest situation (small ion current limit) where incipient ion evaporation effects can be computed in a Taylor cone. An incompatibility between measured and expected ion currents then arises that we cannot explain based on the deficiencies of the experimental system. A review of the possible pitfalls of the theory suggests that the criterion used for ion evaporation to have no effect on the calculation of the field is inadequate. It is apparently not enough for the ion current to be small compared to the jet current. Because the ion current is ejected locally in the narrow region where the electric field is maximum, while the jet current is incorporated into the surface over the wider structure of the meniscus tip, the more stringent condition must be met that the current density of ions evaporating into the vacuum must be much smaller than the current density reaching the interface from the interior of the liquid. This criterion unfortunately cannot be met with the present experimental system.

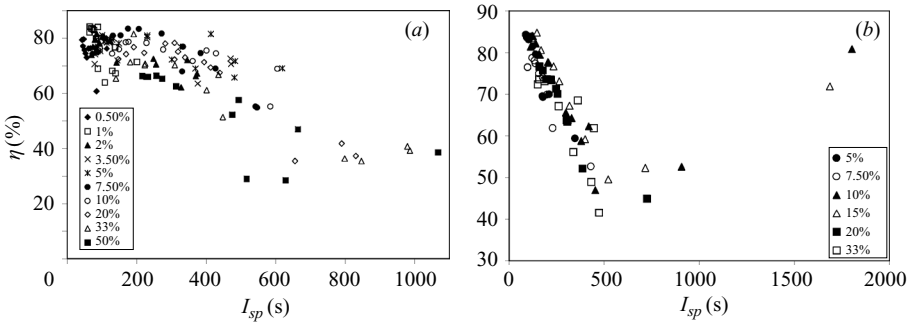

FIGURE 6. Propulsion efficiency versus specific impulse for the two mixtures investigated: (*a*) EMI-BF_4/PC, (*b*) EMI-IM/PC.

5. Propulsive characteristics of PC/ionic liquid mixtures

In addition to their basic interest in the physics of ion evaporation, the unique emissions from the liquids studied makes them also of practical interest. We shall therefore analyse in this section the propulsive characteristics of these mixtures.

The TOF curves of figures 2 and 3 provide a distribution of arrival times for the charged particles contained in the spray. If one knows the kinetic energy per unit charge of these particles, V_a, one can infer all relevant propulsive variables associated with the spray. Prior measurements have shown that V_a is typically close to the needle voltage, with a small voltage drop of 100 to 200 V associated irreversibilities, such as electrical conduction in the liquid (Gamero-Castaño & Hruby 2001, 2002; Bocanegra *et al.* 2004). Because typical needle voltages are 2 kV, these losses are relatively small. We have therefore not repeated these measurements of V_a here but simply assumed that it is 200 V below the needle voltage V. The following integrals of the TOF curves $i(t)$ then yield the flow rate Q, the thrust, the specific impulse I_{sp} (g is the Earth's gravitational acceleration) and the propulsive efficiency η of the spray:

$$\rho Q = \frac{4V_a}{L^2}\int_0^\infty i(t)t\,\mathrm{d}t, \quad \text{Thrust} = \frac{2V_a}{L}\int_0^\infty i(t)\,\mathrm{d}t \tag{5.1a, b}$$

$$I_{sp} = \frac{\text{Thrust}}{\rho Q g}, \quad \eta = \frac{(\text{Thrust})^2}{2\rho Q V_a i(0)} = \frac{\left(\int_0^\infty i(t)\,\mathrm{d}t\right)^2}{2i(0)\int_0^\infty i(t)t\,\mathrm{d}t}. \tag{5.1c, d}$$

Figure 6 plots propulsion efficiency versus specific impulse for the two kinds of mixtures investigated, showing a general initial reduction of the propulsion efficiency with increasing specific impulse. This performance deterioration is associated initially with a loss of sharpness in the mass/charge distribution (TOF curve). The efficiency is expected to become high again in the pure ion evaporation limit at the highest specific impulses reached, as seen in the case of the PC/EMI-Im mixtures. The largest I_{sp} attained, about 2000 s, is the highest so far reported for electrolytes of neutral solvents. In fact, it is remarkable that a single propellant such as 10 % (vol) EMI-Im in PC can span, at varying flow rates, the range of specific impulses from about 100 s up to 2000 s. However, note the small values of the thrust level obtained per Taylor cone, particularly at high specific impulses. This can be seen in table 5, as well as in figure 7 in the form of thrust versus specific impulse curves for both types of mixture.

I (nA)	E_k (V nm^{-1})	I_i (nA)	ρQ (Kg s^{-1})	Thrust (μN)	I_{sp} (s)	η % —	Ψ —	$\ln(I_i \Psi^{13/2})$ (I_i in nA)
148	0.532	0	4.09×10^{-10}	0.456	114	85.8	34.66	
147	0.553	0	3.26×10^{-10}	0.406	127	85.7	35.32	
131	0.587	1	2.27×10^{-10}	0.316	142	84.1	36.40	23.36
114	0.631	4	1.47×10^{-10}	0.235	163	82.3	37.75	24.99
90	0.713	6	7.05×10^{-11}	0.142	205	79.2	40.13	25.79
82	0.755	10	5.03×10^{-11}	0.112	228	76.7	41.27	26.48
69	0.860	13	2.29×10^{-11}	0.0672	299	71.5	44.07	27.17
66	0.905	17	1.69×10^{-11}	0.0547	329	67.0	45.19	27.61
58.6	0.986	21.6	1.01×10^{-11}	0.0376	380	59.8	47.18	28.13
57	1.02	22	8.25×10^{-12}	0.0339	419	61.2	47.99	28.26
47	1.11	26	5.06×10^{-12}	0.0225	454	53.4	49.98	28.69
47	1.38	36	1.34×10^{-12}	0.0119	908	56.4	55.85	29.73
35.4	1.71	31.4	3.66×10^{-13}	0.00647	1800	80.9	62.21	30.30

TABLE 5. Characteristics of sprays 10 % EMI-Im in PC. $V = 2$ kV; V_a taken to be 1.8 kV.

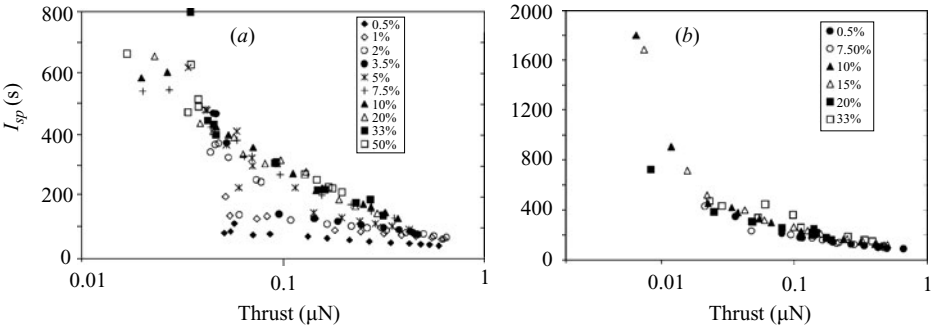

FIGURE 7. Specific impulse versus thrust for the two kinds of mixtures investigated: (*a*) EMI-BF_4/PC, (*b*) EMI-IM/PC.

Evidently, a high degree of multiplexing would be required to attain thrust levels of practical relevance.

6. Conclusions

A study of the emissions of Taylor cones of propylene carbonate seeded with the ionic liquid 1-ethyl-3-methylimidazolium bis(trifluoromethylsulfonyl)imide (EMI-Im) has revealed the cleanest transition so far observed for a single liquid from the pure colloidal regime (drops only) to an almost pure ionic regime. This exceptional situation has permitted the measurement of ion currents very close to the threshold for ion evaporation. Combined with a recently developed method to compute accurately and realistically the complete structure of the cone–jet, we have been able to compare predicted with observed ion current vs. flow rate characteristics. Unfortunately, a variety of limitations noted both in the experimental method and the computational model has precluded a reliable inference of the kinetics of ion evaporation. In fact, a comparison of measured ion currents with predictions from ion evaporation theory yields an anomalously low activation energy. The propulsion characteristics of some of the mixtures analysed are also of considerable practical interest.

Contributions to this work by M. Espina-Trigo, V. Fasson, B. Jorns, D. Garoz and I. Romero-Sanz, and financial support from the US AFOSR through contracts Nos. F-49620-01-1-0416 and FA9550-06-1-0104, and from the Spanish projects DPI2004-05246-C04-02 (MEC) and R05/9961 (CM/UPM) are gratefully acknowledged.

REFERENCES

Barrero, A., Gañán-Calvo, A. M., Dávila, J., Palacios, A. & Gómez-González, E. 1999 The role of the electrical conductivity and viscosity on the motions inside Taylor cones. *J. Electrostatics* **47**, 13–26.

Barrero, A., Lopez-Herrera, J. M., Boucard, A., Loscertales, I. G. & Marquez, M. 2004 Steady cone–jet electrosprays in liquid insulator baths. *J. Colloid Interface Sci.* **272**, 104–108.

Bocanegra, R., Fernandez de la Mora, J. & Gamero-Castaño, M. 2004 Ammonium electrolytes quench ion evaporation in colloidal propulsion. *J. Propulsion Power* **20**, 728–735.

Carretero, J. A. 2005 Numerical simulation of a single emitter colloid thruster in pure droplet cone–jet mode. PhD Thesis, MIT.

Chen, D.-R. & Pui, D. Y. H. 1997 Experimental investigation of scaling laws for electrospraying: dielectric constant effect. *Aerosol Sci. Technol.* **27**, 367–380.

Cherney, L. T. 1999 Structure of Taylor cone–jets: limit of low flow rates. *J. Fluid Mech.* **378**, 167–196.

Cloupeau, M. & Prunet-Foch, B. 1989 Electrostatic spraying of liquids in cone–jet mode. *J. Electrostatics* **22**, 135–159.

Cloupeau, M. & Prunet-Foch, B. 1990 Electrostatic spraying of liquids. Main functioning modes. *J. Electrostatics* **23**, 165–184.

Cloupeau, M. & Prunet-Foch, B. 1994 Electrohydrodynamic spraying functioning modes: a critical review. *J. Aerosol Sci.* **25**, 1021–1036.

Cook, K. D. 1986 Electrohydrodynamic mass-spectrometry. *Mass Spectrometry Rev.* **5**, 467–519.

Espina-Trigo, M. A. 2004 Proyecto de Fin de Carrera (Senior Thesis). Polytechnical University, Madrid (Escuela Tecnica Superior de Ingenieros Aeronáuticos).

Fenn, J. B., Mann, M., Meng, C. K., Wong, S. K. & Whitehouse, C. 1989 Electrospray ionization for mass spectrometry of large biomolecules. *Science* **246**, 64–71.

Fernandez de la Mora, J. 2007 The fluid dynamics of Taylor cones. *Annu. Rev. Fluid Mech.* **39**, 217–243.

Fernandez de la Mora, J. & Loscertales, I. G. 1994 The current emitted by highly conducting Taylor cones. *J. Fluid Mech.* **260**, 155–184.

Fernandez de la Mora, J., Navascués, J., Fernández, F. & Rosell-Llompart, J. 1990 Generation of submicron monodisperse aerosols in electrosprays. *J. Aerosol Sci.* **21**, S673–S676.

Fernandez de la Mora, J., Thomson, B. & Gamero-Castaño, M. 2005 Tandem mobility mass spectrometry study of electrosprayed $Heptyl_4N^+Br^-$ clusters. *J. Am. Soc. Mass Spectrom.*, **16**, 717–732.

Gamero-Castaño, M. & Fernandez de la Mora, J. 2000*a* Direct measurement of ion evaporation kinetics from electrified liquid surfaces. *J. Chem. Phys.* **113**, 815–832.

Gamero-Castaño, M. & Fernandez de la Mora, J. 2000*b* Kinetics of small ion evaporation from the charge and size distributions of multiply charged electrospray clusters. *J. Mass Spectrometry* **35**, 790–803.

Gamero-Castaño, M. & Hruby, V. 2001 Electrospray as a source of nanoparticles for efficient colloid thrusters. *J. Propulsion Power* **17**, 977–987.

Gamero-Castaño, M. & Hruby, V. 2002 Electric measurements of charged sprays emitted by cone–jets. *J. Fluid Mech.* **459**, 245–276.

Gañán-Calvo, A. 1997 cone–jet analytical extension of Taylor's electrostatic solution and the asymptotic universal scaling laws in electrospraying. *Phys. Rev. Lett.* **79**, 217–220.

Gañán-Calvo, A. M. 1999 The surface charge in electrostatic spraying: its nature and its universal scaling laws. *J. Aerosol Sci.* **30**, 863–872.

Gañán-Calvo, A. M. 2004 On the general scaling theory for electrospraying. *J. Fluid Mech.* **507**, 203–212.

Gañán-Calvo, A. M., Dávila, J. & Barrero, A. 1997 Current and droplet size in the electrospraying of liquids. Scaling laws. *J. Aerosol Sci.* **28**, 249–275.

Higuera, F. J. 2003*a* Flow rate and electric current emitted by a Taylor cone. *J. Fluid Mech.* **484**, 303–327.

Higuera, F. J. 2003*b* Ion evaporation from the surface of a Taylor cone. *Phys. Rev.* E **68**, 016304.

Higuera, F. J. 2004 Liquid flow induced by ion evaporation in an electrified meniscus. *Phys. Rev.* E **69**, 066301.

Huberman, M. N. 1970 Measurement of the energy dissipated in the electrostatic spraying process. *J. Appl. Phys.* **41**, 578–584.

Huberman, M. N. & Rosen, S. G. 1974 Advanced high-thrust colloid sources. *J. Spacecraft* **11**, 475–480.

Iribarne, J. V. & Thomson, B. A. 1976 On the evaporation of small ions from charged droplets. *J. Chem. Phys.* **64**, 2287–2294.

Ku, B. K. & Fernandez de la Mora, J. 2004 Ion evaporation kinetics of tetra-alkylammonium salts in formamide solution. *J. Phys. Chem.* B **108**, 14915–14923.

Landau, L. D. & Lifshitz, E. M. 1960 *Electrodynamics of Continuous Media,* Chap. 2. Pergamon.

Loscertales, I. G. & Fernandez de la Mora, J. 1995 Experiments on the kinetics of field-evaporation of small ions from droplets. *J. Chem. Phys.* **103**, 5041–5060.

Lozano, P. 2003 Studies on the ion-droplet mixed regime in colloid thrusters. PhD Thesis, MIT.

Lozano, P. & Martinez-Sanchez, M. 2005 Ionic liquid ion sources: characterization of externally wetted emitters. *J. Colloid Interface Sci.* **282**, 415–421.

Martinez-Sanchez, M., Fernandez de la Mora, J., Hruby, V, Gamero-Castaño, M. & Khayms, V. 1999 Research on colloid thrusters. *26th Intl Electric Propulsion Conference, Kitakyushu, Japan*, pp. 93–100. Electric Rocket Propulsion Society.

McEwen, A. B., Ngo, H. L., LeCompte, K. & Goldman, J. L. 1999 Nonaqueous electrolytes for electrochemical capacitors: Imidazolium cations and inorganic fluorides with organic carbonates. *J. Electrochem. Soc.* **146**, 1687–1995.

Notz, P. K. & Basaran, O. A. 1999 Dynamics of drop formation in an electric field. *J. Colloid Interface Sci.* **213**, 218–237.

Perel, J., Mahoney, J. F., Moore, R. D. & Yahiku, A. Y. 1969 Research and development of a charged-particle bipolar thruster. *AIAA J.* **7**, 507–511.

Prewett, P. D. & Mair. G. L. R. 1991 *Focused Ion Beams from LMIS*. Wiley.

Reznik, S. N., Yarin, A. L., Theron, A. & Zussman, E. 2004 Transient and steady shapes of droplets attached to a surface in a strong electric field. *J. Fluid Mech.* **516**, 349–377.

Riddick, J. A., Bunger, W. B. & Sakano, T. K. 1986 *Organic Solvents*, Vol. 11, 4th Edn, Wiley.

Romero-Sanz, I., Aguirre-de-Carcer, I. & Fernandez de la Mora, J. 2005 Ionic propulsion based on heated Taylor cones of ionic liquids. *J. Prop. Power* **21**, 239–242.

Romero-Sanz, I., Bocanegra, R., Fernandez de la Mora, J. & Gamero-Castaño, M. 2003 Source of heavy molecular ions based on Taylor cones of ionic liquids operating in the pure ion evaporation regime. *J. Appl. Phys.* **94**, 3599–3605.

Romero-Sanz, I. & Fernandez de la Mora. J. 2004 Spatial structure and energy distribution of electrosprays of ionic liquids in vacuo. *J. Appl. Phys.* **95**, 2123–2129.

Rosell-Llompart, J. & Fernandez de la Mora, J. 1994 Generation of monodisperse droplets 0.3 to 4 μm in diameter from electrified cone–jets of highly conducting and viscous liquids. *J. Aerosol Sci.* **25**, 1093–1119.

Saville, D. A. 1997 Electrohydrodynamics: The Taylor-Melcher leaky dielectric model. *Annu. Rev. Fluid Mech.* **29**, 27–64.

Taylor, G. I. 1964 Disintegration of water drops in an electric field. *Proc. R. Soc. Lond.* A **280**, 383–397.

Zeleny, J. 1917 Instability of electrified liquid surfaces. *Phys. Rev.* **10**, 1–6.